Wuhan University
Journal of Natural Sciences

2022, Vol.27 No.1, 063-067

Article ID 1007-1202(2022)01-0063-05
DOI https://doi.org/10.1051/wujns/2022271063

Quenching Fluorescence of Quantum Dots by Using Gold Nanocrystals in Quantum and Classical Size Regime

☐ WANG Peng[1*], ZHOU Tao[2*], DING Sijing[2†], LI Jianbo[3], WANG Ququan[4†]

1. School of Electronic Engineering and Intelligent Manufacturing, Anqing Normal University, Anqing 246133, Anhui, China;

2. School of Mathematics and Physics, China University of Geosciences (Wuhan), Wuhan 430074, Hubei, China;

3. Institute of Mathematics and Physics, Central South University of Forestry and Technology, Changsha 410004, Hunan, China;

4. School of Physics and Technology, Wuhan University, Wuhan 430072, Hubei, China

Abstract: This paper investigates the factors which can influence the quenching effect from the perspective of energy transfer. The quenched fluorescence of the CdSe semiconductor quantum dots (SQDs) by using plasmonic Au nanocrystals (p-AuNCs) and molecule-like Au nanocrystals (m-AuNCs) in aqueous suspensions and spin-coated films is comparatively investigated. In the aqueous suspensions, the p-AuNCs have larger quenching effect than the m-AuNCs. In the spin-coated films, the p-AuNCs and m-AuNCs have comparable quenching factor. Furthermore, the experiments show that the p-AuNCs simultaneously enhance the radiative and nonradiative rates. But the m-AuNCs only enhance the nonradiative rate of the SQDs, which reveals the difference of quenching process between the p-AuNCs and m-AuNCs. This result of the research has guiding significance for the detection technique based on the fluorescence quenching.

Key words: fluorescence quenching; energy transfer; plasmons; nanocluster

CLC number: O 232; O 193

Received date: 2021-08-16

Foundation item: Supported by the Natural Science Foundation of Educational Commission of Auhui Province of China (KJ2019A0567), the National Natural Science Foundation of China (11904332), the Natural Science Foundation of Zhejiang Province (LQQ20A040001), Hubei Key Laboratory of Optical Information and Pattern Recognition by Wuhan Institute of Technology (202004), Hunan Provincial Natural Science Foundation (2020JJ4935), and Scientific Research Fund of Hunan Provincial Education Department (20B602)

Biography: WANG Peng, male, Associate professor, research direction: electronic system. E-mail: wangp@aqtc.edu.cn

†To whom correspondence should be addressed. E-mail: dingsijing@cug.edu.cn; qqwang@whu.edu.cn

*These authors contributed equally to this work

0 Introduction

In recent years, noble metal nanocrystals have attracted greatly-increasing interests from researchers because of their unique properties. In materials science, the structure of material determines the material properties, and the various preparation methods of noble metal nanocrystals provide possibilities for materials that can adapt to different functional requirements[1-3]. Therefore, the researchers are committed to research the noble metal nanocrystals which have tunable optical response by adjusting their surface factors such as size, shape, and component[4-10], which leads to diverse applications ranging from surface enhanced Raman scattering, bio-imaging, photothermal cancer treatment, photocatalysis, to ultrafast optical information processing[11-14]. Especially, the unique optical responses of the Au and Ag nanocrystals (AuNCs and AgNCs) in the quantum size regime have been made many practical achievements[15-18]. For instance, the plasmon resonance wavelength of the individual ligand-free AgNCs blue-shifts 500 meV as the nanocrystals' diameter decreases from 20 nm to less than 2 nm, which is revealed to be caused by the prominently increased quantum confinement effect in the quantum-sized nanocrystals[19-22].

Noble metal nanocrystals with strong plasmon resonance are widely used to tune optical emission behaviors of the nearby nanoemitters. Fluorescence detection technology is an effective tool in the communities of biomedicine and geological exploration, the luminescence modulation process of which has always been an important subject. For the metal surface plasma has significant extinction and field enhancement effects, the fluorescence could be largely enhanced or significantly quenched by the metal

nanocrystals depending on the competition of the enhanced radiative and nonradiative processes, which can be controlled by adjusting the size of metal nanocrystals or the separation distance between metal nanocrystals and nanoemitters[23-26]. When the size of the metal nanocrystals decreases to very small, the plasmon resonance disappears and the molecule-like behavior of the atomic clusters exhibits. The molecule-like metal nanocrystals could not be used to enhance emission of the nearby optical emitters but could be used to quench fluorescence and have also prospective applications in bio-sensor[27-29].

In our previous studies, we observed the non-monotonic shift in the spectrum of AuNCs ranging from the classical to the quantum size, due to the competition between quantum and classical effect[30]. Because of the different performance of AuNCs in quantum and classical size, we design the fluorescence quenching experiment of AuNCs in these two size regions, respectively. In this paper, we investigate fluorescence of CdSe SQDs quenched by plasmonic Au nanocrystals (p-AuNCs) and molecule-like Au nanocrystals (m-AuNCs) in aqueous suspensions and solid films. We find that both p-AuNCs and m-AuNCs exhibits strong quenching effect, but there are essential differences in quenching modes between p-AuNCs and m-AuNCs. After analyzing the experimental data, our results have shown that the p-AuNCs enhance both radiative and nonradiative rates but the m-AuNCs only enhance nonradiative rate of the SQDs.

1 Materials and Methods

CdSe SQDs with the central emission wavelengths of ~655 nm are purchased from Invitrogen Corporation. The m-AuNCs and p-AuNCs were prepared by thermal etching the same concentration of Au nanorod solution according to a previously reported work by our team[30]. We found that the size of AuNCs is solely depended on the reaction temperature. The m-AuNCs and p-AuNCs are prepared by adjusting the etching temperature to 260 ℃ and 205 ℃, respectively. The CdSe SQDs and AuNCs are mixed to form suspensions. The concentration of m-AuNCs in the mixed suspensions is adjusted by the volume (V_{Au}) of aqueous liquid of m-AuNCs. The complex film consisting of the CdSe SQDs and the p-AuNCs or m-AuNCs are prepared by spin-coating mixed suspensions.

The transmission electron microscopy (TEM) images and high-resolution TEM images are performed by a JEOL 2010 HT and JEOL 2010 field effect transistor TEM at an accelerating voltage of 200 kV, respectively. The extinction spectrum is recorded by a TU-1810 UV-Vis-NIR spectrophotometer. The fluorescence spectrum excited by a Xe lamp is recorded by a Hitachi F-4500 fluorescence spectrophotometer. The fluorescence signal excited by a laser is collected in reflection geometry, filtered with two filters and recorded by a spectrometer (Spectrapro 2500i, Acton) with a liquid-nitrogen-cooled charge-coupled device (SPEC-10, Princeton). The time-resolved fluorescence emission decay traces are recorded by using a time-correlated single-photon counting system (PicoQuant GmbH), and the pulsed laser is provided by a mode-locked Ti: Sapphire laser (Mira 900, Coherent) equipped with an optical frequency doubling system.

2 Results

The TEM images of the p-AuNCs and m-AuNCs are shown in Fig. 1(a) and 1(b), respectively. The p-AuNCs have an average size of ~34 nm and strong resonance absorption at the wavelength of 528 nm (Fig. 1(c)). On the contrary, the quantum-sized m-AuNCs have a very small diameter of ~2 nm, which have an absorption band edge around 500 nm and the plasmon resonance absorption around 530 nm is efficiently suppressed (see Fig. 1(c)). The excitonic absorption band edge of the CdSe SQDs around 630 nm is also shown in Fig. 1(c).

In our experiment, the relationship between the quenching effect and the concentration of AuNCs was investigated (Fig. 2). The fluorescence of CdSe SQDs was almost completely quenched by a small amount of p-AuNCs. Therefore, only the experimental data of m-AuNCs are shown below. Figure 2(a) clearly demonstrates that the fluorescence of the suspended CdSe SQDs is quenched by the m-AuNCs. It is shown that the quenching effect has an analogous logarithmic relationship with the concentration of metal solution. The quenching efficiency is defined as $q = 1-I_{FL}/I_{FL,0}$, where I_{FL} and $I_{FL,0}$ are the SQDs' fluorescence peak intensity with and without AuNCs, respectively. The volume of m-AuNCs (V_{Au}) added to the SQDs are 0, 5, 10, 20, 30, 40, 50, 70, 100, 150, 200, 300, and 400 μL. The q values dramatically increase from 0 to 0.58 as V_{Au} increases from 0 to 40 μL, and then slowly increases to 0.81 as V_{Au} further increases to 400 μL (see the inset in Fig. 2(a)). As the number of AuNCs increases, there are more absorption cross sections in the system. The quenching effect in-

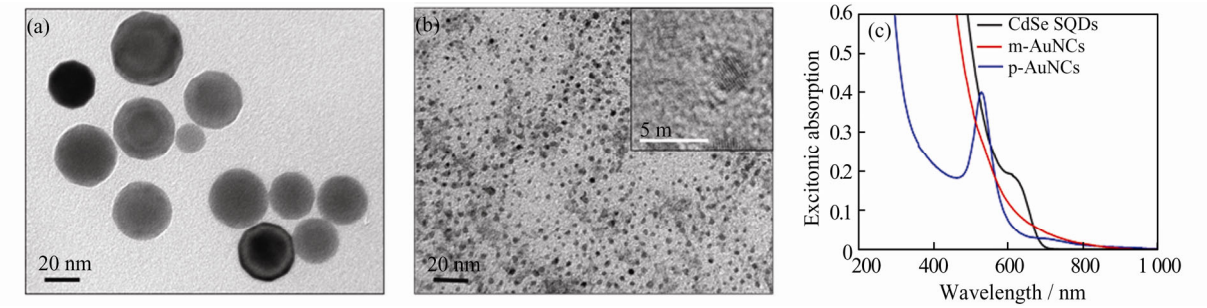

Fig. 1 Nanostructure and absorption spectra of p-AuNCs and m-AuNCs

(a) TEM image of p-AuNCs with average diameter of ~34 nm; (b) TEM image of m-AuNCs with average diameter of ~2 nm; (c) Absorption spectra of p-AuNCs and m-AuNCs. Emcitonic absorption band edge of CdSe SQDs is located at 630 nm

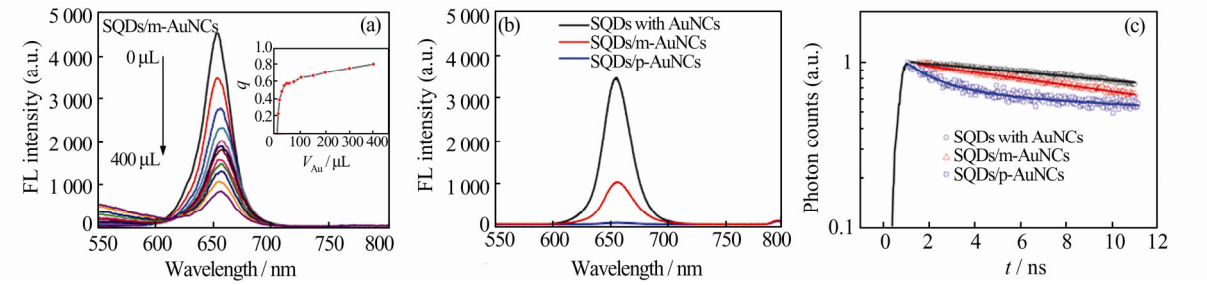

Fig. 2 Quenching fluorescence of CdSe SQDs by p-AuNCs and m-AuNCs in suspensions

(a) Quenched fluorescence spectra of SQDs with different amounts of m-AuNCs. The variance of quenching efficency with the V_{Au} is shown in the illustration. Quenched fluorescence spectra (b) and normalized TRFL (c) of SQDs with p-AuNCs or m-AuNCs

creased with the increase of concentration can be attributed to the increase of whole absorption cross section. As comparison, the p-AuNCs exhibits stronger quenching effect than the m-AuNCs and the corresponding q value reaches as high as 0.95 (see Fig. 2(b)).

To investigate the physical mechanism of the fluorescence quenched by the p-AuNCs and m-AuNCs, the time-resolved fluorescence (TRFL) of the CdSe SQDs with and without AuNCs is recorded at the central emission wavelength of the SQDs at 655 nm. As shown in Fig. 2(c), the bare CdSe SQDs have a single exponential decay, with decay rate $\Gamma_0 \approx 0.030\ 6\ \text{ns}^{-1}$. The SQDs with m-AuNCs also exhibit a single exponential decay, but the decay rate Γ increases to $0.044\ 6\ \text{ns}^{-1}$. This indicates that all SQDs are coupled to the small-sized m-AuNCs. The fluorescent group of quantum dots is regarded as a pair of dipoles, and the electromagnetic field generated by them interacts with the m-AuNCs, which is accompanied by the nanosurface energy transfer (NSET). The energy transfer rate is approximately estimated by the relation, $\Gamma_{ET} = \Gamma - \Gamma_0 = 0.014\ \text{ns}^{-1}$.

On the contrary, the SQDs with p-AuNCs have two-exponential decay processes, which can be fitted by

$$I_{TRFL}(t) = A_f e^{-t/\tau_f} + A_s e^{-t/\tau_s} \quad (1)$$

where A_f (A_s) and τ_f (τ_s) represent weight factor and the lifetime of the fast (slow) decay processes, respectively. From Fig. 2(c), we obtained $\tau_f = 1.4$ ns, $\tau_s = 38.1$ ns, $A_f/(A_f + A_s) = 0.31$, and $A_s/(A_f + A_s) = 0.69$. The lifetime of the slow process τ_s is very close to that of the bare SQDs, which indicates this slow decay process is attributed to the SQDs uncoupled to p-AuNCs. Except for the slow decay of quantum dots, the curve of fluorescence life shows a fast decay process which is attributed to the SQDs strongly coupled to p-AuNCs. This leads to a very strong coupling energy transfer. The energy transfer rate is approximately estimated by $\Gamma_{ET} = 1/\tau_f - \Gamma_0 \approx 0.683\ \text{ns}^{-1}$.

The fluorescence quenching effect is strongly dependent on the complex nanostructure of the metal nanocrystals and the optical nanoemitters. Then, we further investigate the fluorescence behaviours of the complex films consisting of CdSe SQDs and p-AuNCs or m-AuNCs. The film samples are prepared by spin-coating of the complex suspensions onto the fused quartz substrate. Figure 3(a) and 3(b) presents quenched fluorescence spectra and TRFL of the bare CdSe SQDs and those with p-AuNCs or m-AuNCs.

In the complex film, the p-AuNCs have weaker quenching effect ($q = 0.79$) than the ones in the suspensions,

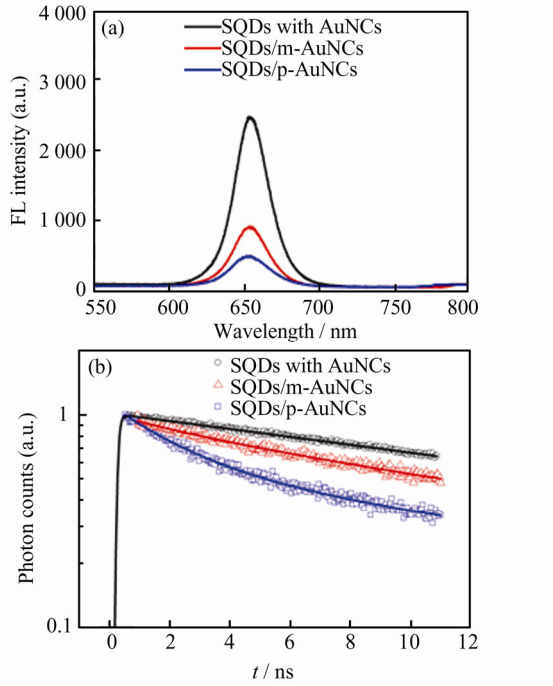

Fig. 3 Quenching fluorescence spectra (a) and normalized TRFL (b) of CdSe SQDs by p-AuNCs and m-AuNCs in complex film

the fast decay rate slightly decreases to 0.370 3 ns^{-1}, the slow decay rate increases to 0.041 2 ns^{-1}, and the corresponding weight factor $A_f/(A_f + A_s)$ increases to 0.5 (more detailed data are presented in Table 1). Since the total decay rate Γ is the sum of the radiative and nonradiative rate ($\Gamma = \gamma_{rad} + \gamma_{nonrad}$), and the fluorescence intensity is proportional to the radiative rate γ_{rad}, therefore, the relatively smaller quenching factor with comparable decay rates in the complex films can be explained by the plasmon-enhanced radiative rate[31]. Part of the energy transferred to the gold nanoparticles drives the plasma state. The electrons emit photons in the transition process of the plasmon state to the ground state. The radiation of photon can reduce the quenching effect.

On the other hand, there is no plasmon enhancement on the radiative rate of the SQDs' fluorescence when the m-AuNCs are used, which result in a prominent quenching effect with one-component exponential decay fluorescence of the CdSe SQDs with m-AuNCs in both aqueous suspensions and complex films.

Table 1 Fluorescence decay parameters of SQDs

Item	Sample	q	τ_f/ns	τ_s/ns	$\frac{A_f}{A_f + A_s}$
Suspension	SQDs	—	—	32.7	0
	SQDs/m-AuNCs	0.69	—	22.4	0
	SQDs/p-AuNCs	0.97	1.4	38.1	0.31
Film	SQDs	—	—	23.4	0
	SQDs/m-AuNCs	0.62	—	15.9	0
	SQDs/p-AuNCs	0.79	2.7	24.3	0.50

3 Conclusion

In summary, we comparatively investigate the quenched fluorescence of the CdSe SQDs by p-AuNCs and m-AuNCs in the suspensions and complex films. In both suspensions and films, the m-AuNCs have comparable quenching effect (q values are about 0.69 and 0.62 respectively), and the quenched fluorescence of the SQDs follows a single exponential decay process. On the other hand, the p-AuNCs demonstrate stronger quenching effect than the m-AuNCs. The fluorescence quenching factor of the SQDs with p-AuNCs reaches as high as 0.97 in the suspensions. The prominent two-decay processes induced by plasmon-enhanced radiative rate are observed in the complex films. These observations could provide an alternative route to the prospective applications in bio-sensing and bio-labeling.

Acknowledgments

The authors thank NAN Fan and DU Taoyuan for the helpful discussions.

References

[1] Burda C, Chen X B, Narayanan R, *et al*. Chemistry and properties of nanocrystals of different shapes [J]. *Chem Rev*, 2005, **105**(27): 1025-1102.

[2] Cui M L, Zhao Y, Song Q J. Synthesis, optical properties and applications of ultra-small luminescent gold nanoclusters [J]. *Trends Anal Chem*, 2014, **57**: 73-82.

[3] Tao R, Habas S, Yang P D. Shape control of colloidal metal nanocrystals [J]. *Small*, 2008, **4**(3): 310-325.

[4] Link S, El-Sayed M A. Shape and size dependence of radiative, non-radiative and photothermal properties of gold nanocrystals [J]. *Phys Chem*, 2000, **19**(3): 409-453.

[5] Xia Y N, Xiong Y J, Lim B, *et al*. Shape-controlled synthesis of metal nanocrystals: Simple chemistry meets complex physics? [J]. *Angew Chem Int Ed*, 2009, **38**(1): 60-103.

[6] Xiong Y J, Xia Y N. Shape-controlled synthesis of metal nanostructures: The case of palladium [J]. *Adv Mater*, 2007, **19**(20): 3385-3391.

[7] Link S, El-Sayed M A. Size and temperature dependence of the plasmon absorption of colloidal gold nanoparticles [J]. *J Phys Chem B*, 1999, **103**: 4212-4217.

[8] Pelton M, Aizpurua J, Bryant G. Metal-nanoparticle plasmonics [J]. *Laser Photonics Rev*, 2008, **2**(3): 136-159.

[9] Gong L, Qiu Y, Nan F, *et al*. Synthesis and largely enhanced nonlinear refraction of Au@Cu_2O core-shell nanorods [J]. *Wuhan Univ J Nat Sci*, 2018, **23**(5): 418-423.

[10] Zhang Y, Li X H, Peng C X. Modification of photoluminescence properties of ZnO island films by localized surface plasmons [J]. *Chin Phys Lett*, 2012, **29**(10): 107803.

[11] Chithrani B D, Ghazani A A, Chan W C W. Determining the size and shape dependence of gold nanoparticle uptake into mammalian cells [J]. *Nano Lett*, 2006, **6**(4): 662-668.

[12] Jain P K, Huang X H, El-Sayed I H, *et al*. Review of some interesting surface plasmon resonance-enhanced properties of noble metal nanoparticles and their applications to biosystems [J]. *Plasmonics*, 2007, **2**(3): 107-118.

[13] Austin L A, Mackey M A, Dreaden E C, *et al*. The optical, photothermal, and facile surface chemical properties of gold and silver nanoparticles in biodiagnostics, therapy, and drug delivery [J]. *Arch Toxicol*, 2014, **88**(7): 1391-1417.

[14] Liu J, Sheng X, Huang B, *et al*. Optimization of surface plasmon resonance sensor based on multilayer film structure [J]. *Wuhan Univ J Nat Sci*, 2020, **25**(4): 352-358.

[15] Farrag M, Tschurl M, Heiz U. Chiral gold and silver nanoclusters: preparation, size selection, and chiroptical properties [J]. *Chem Mater*, 2013, **25**(6): 862-870.

[16] Aldeek F, Muhammed M A H, Palui G, *et al*. Growth of highly fluorescent polyethylene glycol- and zwitterion-functionalized gold nanoclusters [J]. *ACS Nano*, 2013, **7**(3): 2509-2521.

[17] Mishra D, Lobodin V, Zhang C, *et al*. Gold-doped silver nanoclusters with enhanced photophysical properties [J]. *Phys Chem Chem Phys*, 2018, **20**(18): 12992-13007.

[18] Zhou T Y, Lin L P, Rong M C, *et al*. Silver-gold alloy nanoclusters as a fluorescence-enhanced probe for aluminum ion sensing [J]. *Anal Chem*, 2013, **85**(20): 9839-9844.

[19] Peng S, McMahon J M, Schatz G C, *et al*. Reversing the size-dependence of surface plasmon resonances [J]. *Proc Natl Acad Sci*, 2010, **107**(33): 14530-14534.

[20] Sholl D, Steckel J A. *Density Functional Theory*: *A Practical Introduction* [M]. Hoboken: Wiley-Interscience, 2009.

[21] Genzel L, Martin T P, Kreibig U. Dielectric function and plasma resonances of small metal particles [J]. *Z Phys B Condens Matter*, 1975, **21**(4): 339-346.

[22] Scholl J A, Koh A L, Dionne J A. Quantum plasmon resonances of individual metallic nanoparticles [J]. *Nature*, 2012, **483**(7390): 421-427.

[23] Schneider G, Decher G, Nerambourg N, *et al*. Distance-dependent fluorescence quenching on gold nanoparticles ensheathed with layer-by-layer assembled polyelectrolytes [J]. *Nano Lett*, 2006, **6**(3): 530-536.

[24] Viste P, Plain J, Jaffiol R, *et al*. Enhancement and quenching regimes in metal-semiconductor hybrid optical nanosources [J]. *ACS Nano*, 2010, **4**(2): 759-764.

[25] Jin Y D, Gao X H. Plasmonic fluorescent quantum dots [J]. *Nat Nanotech*, 2009, **4**(9): 571-576.

[26] Shevchenko E V, Ringler M, Schwemer A, *et al*. Self-assembled binary superlattices of CdSe and Au nanocrystals and their fluorescence properties [J]. *J Am Chem Soc*, 2008, **130**(11): 3274-3275.

[27] Dubertret B, Calame M, Libchaber A J. Single-mismatch detection using gold-quenched fluorescent oligonucleotides [J]. *Nat Biotech*, 2001, **19**(4): 365-370.

[28] Chan Y H, Chen J X, Wark S E, *et al*. Using patterned arrays of metal nanoparticles to probe plasmon enhanced luminescence of CdSe quantum dots [J]. *ACS Nano*, 2009, **3**(7): 1735-1744.

[29] Muhammed M A H, Aldeek F, Palui G, *et al*. Growth of in situ functionalized luminescent silver nanoclusters by direct reduction and size focusing [J]. *ACS Nano*, 2012, **6**(10): 8950-8961.

[30] Ding S J, Yang D J, Li J L, *et al*. Nonmonotonous shift of quantum plasmon resonance and plasmon-enhanced photocatalytic activity of gold nanoparticles [J]. *Nanoscale*, 2017, **9**(9): 3188-3195.

[31] Ding S J, Liang S, Nan F, *et al.* Synthesis and enhanced fluorescence of Ag doped CdTe semiconductor quantum dots [J]. *Nanoscale*, 2015, **7**(5): 1970-1976.

□